ELECTRON TRANSFER AT BORON-DOPED DIAMOND ELECTRODES. COMPARISON WITH Pt, Au AND RuO_2

Francesco FRISO and Sergio TRASATTI[1,*]

Department of Physical Chemistry and Electrochemistry, University of Milan, Via Venezian 21, 20133 Milan, Italy; e-mail: [1] sergio.trasatti@unimi.it

Received June 9, 2003
Accepted August 19, 2003

In honour of the colleague and close friend Professor Sergio Roffia on the occasion of his retirement.

Electron exchange reaction rates were compared for boron-doped diamond (BDD), Pt, Au and RuO_2 using $[Ru(NH_3)_6]^{3+/2+}$ as a redox couple. The study was carried out by cyclic voltammetry; calculations were performed by Nicholson's procedure. The results show that the rate constants on BDD, Pt and Au are qualitatively similar, one order of magnitude higher than on RuO_2. The outcome is explained in terms of the specific structure of the interface between oxides and electrolyte solutions.

Keywords: Diamond; Platinum; Gold; Ruthenium; Electrodes; Cyclic voltammetry; Kinetics.

Doped diamond films exhibit very interesting properties from the electrochemical point of view[1,2]: (i) small background currents, (ii) wide potential window and (iii) optimum response to electron exchange reactions. Diamond films can be deposited on different substrates, but the surface response does not appear to be substantially influenced by the nature of the support. Conversely, diamond can be doped with different elements and its properties are reported to depend on the kind and concentration of dopants[3]. The most popular material is boron-doped diamond (BDD) whose properties depend on the procedure of preparation and the amount of doping[4].

A typical requirement for a good electrode is the ability to exchange electrons with a redox system in solution reversibly and with small activation energy. Therefore, diamond electrodes have often been tested using various kinds of redox systems[5–12]. The behavior has been scrutinized as a function of the doping element, of the doping concentration, of the kind of surface pre-treatment, and of the nature of the redox system (outer- *vs* inner-sphere reaction). However, it has been recently pointed out[12] that typical outer-

sphere reactions such as those involving aqua-cations might change to inner-sphere on diamond electrodes because of interactions with surface oxygen-terminated sites on the diamond surface.

Also, the behavior of diamond films is often compared with that of other forms of carbon (*e.g.*, glassy carbon, graphite) rather than with typically metallic surfaces. In addition, calculations of electron exchange rate constants are scarce[3,9,11,12] whereas phenomenological analyses (ΔE_p, I_p, *etc.*) are usually preferred.

In the above context and for the above reasons, the electron exchange ability of boron-doped diamond film electrodes has been investigated in this work using $[Ru(NH_3)_6]^{3+}/[Ru(NH_3)_6]^{2+}$ as a redox system with weak interaction with oxygen-terminated groups, and Pt, Au, and thin RuO_2 films as comparison with electronically conductive surfaces. In particular, crystalline RuO_2 is a true metal, but with a highly hydrophilic surface which is fully covered with OH groups, in contrast to Pt and Au, whose surfaces are relatively hydrophobic below the oxygen adsorption potential range.

EXPERIMENTAL

Boron-Doped Diamond

Plates (10 × 10 cm) of low-resistivity (1–3 mΩ cm), p-type, (100) Si wafers covered on one side with BDD were purchased from CSEM, Neuchatel (Switzerland). The thickness of the diamond film was 1 μm (±10%), the resistivity 15 mΩ cm (±30%), consistent with a B concentration of 3500–3600 ppm.

Electrodes

Platinum. The Pt electrode was a 1 × 1 cm platelet, spot-welded to a Pt wire 0.5 mm in diameter. The wire was then inserted into a Teflon holder so that only the platelet was exposed to the solution. Before each experiment, the Pt surface was pre-treated with wet alumina powder (0.05 μm) and finally carefully rinsed with MilliQ water. The state of the surface was then checked voltammetrically in a H_2SO_4 aqueous solution.

Boron-doped diamond. A piece of 1-cm^2 surface was cut from the as-received sample. A thin copper wire was fixed to the Si-side of the specimen with a silver conducting paste. The whole non-diamond parts were then masked by means of a two-components non-contaminating Epoxy resin (Scotchcast No. 4, 3M). Such a resin was successfully used with Ag single-crystal electrodes to insulate the working surface.

Polycrystalline RuO_2. A film of RuO_2 was deposited on a Ti support by thermal decomposition. Since BDD is exceptionally flat whereas RuO_2 films tend to be highly rough, special care was taken in the preparation of a smooth RuO_2 sample. The Ti support (1 × 1 cm platelet with a 5-cm tiny stem) was polished with emery-paper down to the smallest mesh, then with an aqueous suspension of Al_2O_3. The support was then rinsed with purified water, dried and weighed.

The precursor was a 0.02 M solution of $RuCl_3 \cdot xH_2O$ in a mixture of isopropyl alcohol and 10 wt.% HCl. The solution was brushed onto the Ti surface, the solvent evaporated at 60–80 °C for 3 min, the sample fired in a furnace at 400 °C for 5 min. Before starting a second run, the sample was immersed in an ultrasonic bath (isopropyl alcohol) so as to remove all loosely held particles (the cause of unstable roughness). The operation was repeated until *ca* 1 mg of RuO_2 was deposited on the support. The number of operations needed to reach the final weight was *ca* 70. Finally, the sample was subject to a stabilizing annealing of 1 h at 400 °C. The sample was then mounted in a Teflon holder as described elsewhere[13].

Solutions

The $[Ru(NH_3)_6]^{3+}/[Ru(NH_3)_6]^{2+}$ redox system was used as a typical outer-sphere reaction. $RuCl_3(NH_3)_6$ (Aldrich) was used as received without further purification. Distilled water was purified in a MilliQ apparatus. Solutions were prepared volumetrically.

Cell

The four-compartment cell (working electrode, two counter-electrodes (Pt) and reference electrode) was described elsewhere[14]. Ohmic drops were minimized with a Luggin capillary. Solutions were deaerated before each experiment by bubbling purified nitrogen for at least 30 min.

Reference Electrode

Potentials were measured and are reported *vs* SCE reference electrode.

Instrumentation

A 2051 AMEL potentiostat/galvanostat model coupled with a 567 AMEL function generator was used for cyclic voltammetry and steady-state polarization curves. Potentials were read on a 631 AMEL electrometer. Experimental curves were recorded using a LY1600 Lynseis X-Y recorder.

Pre-Treatments

Pt and RuO_2 electrodes were pre-treated by cycling the electrode potential within specific limits until the "standard" voltammetric curves were observed. These limits were –0.2 and 1.15 V for Pt, and 0.15 and 1.15 V for RuO_2. In the case of BDD, an oxygen-terminated surface[15] was prepared by anodically polarizing the electrodes in 0.5 M H_2SO_4 for 30 min at 10 mA cm^{-2} (geometric surface).

RESULTS AND DISCUSSION

BDD films prepared by chemical vapor deposition as for the samples in this work, exhibit a H-terminated surface with hydrophobic properties[8]. If polarized anodically, the surface is changed into a O-terminated surface with hydrophilic characteristics. In view of the comparison with Pt and RuO_2,

the BDD samples used in this work were converted before use so as to work with a surface chemically closer to those of the other two materials.

Anodic Pre-Treatment of BDD

As recommended in the literature[16,17], BDD samples were subjected to anodic polarization for 30 min at 10 mA cm^{-2} in aqueous 0.5 M H_2SO_4. For the purpose of giving evidence of surface modifications, chronopotentiometric curves were recorded at current densities 10 μA cm^{-2}–10 mA cm^{-2} before and after the anodic pre-treatment. The results are shown in Fig. 1. The main differences between the two families of curves are: (i) At the same current density, the plateau reached by the potential is at more positive values

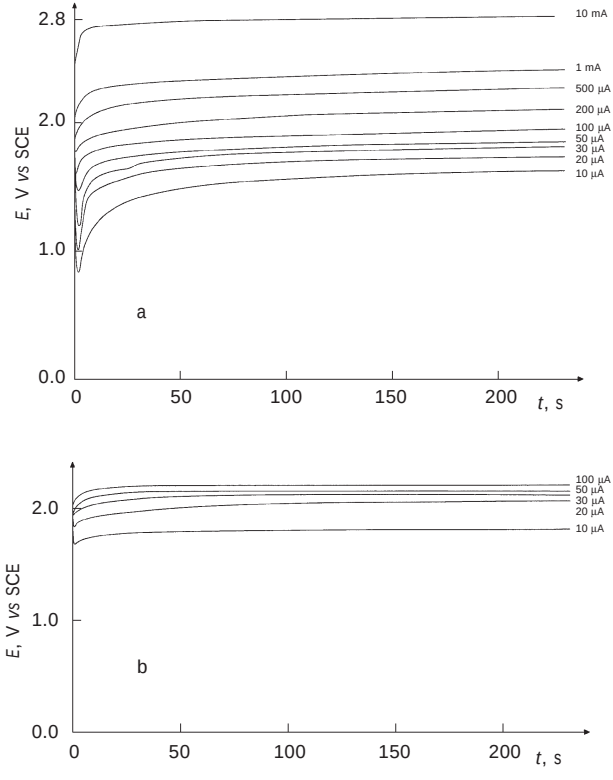

FIG. 1
Potential–time curves of BDD electrodes in 0.5 M H_2SO_4. The applied current is indicated by the curves. Before (a), and after 30 min (b) of anodic treatment in the same solution at 10 mA cm^{-2}

after anodization. (ii) The curves exhibit an induction time before anodization which disappears after the anodic treatment. In both cases, after a few seconds of polarization, the potential stays remarkably constant. This indicates that the processes occurring on the surface during anodic charging is not simply double-layer charging otherwise a steady increase of potential would be observed. Rather, anodic processes are taking place. Before polarization (Fig. 1a), such processes are certainly related to oxidation of the H-terminated surface. After polarization (Fig. 1b), since it is reported that conversion to O-terminated surfaces is only partial, surface oxidation processes are continuing although on a smaller fraction of the surface, whereas deeper oxidation can take place at some specific sites (see later on). In both cases it is definitely argued that capacitive currents are very small, much smaller than those usually attributed to metallic surfaces.

Cyclic Voltammetry in "Blank" Solution

Cyclic voltammetric curves were recorded in aqueous 0.5 M H_2SO_4 starting from a potential window of 0.2 V from –0.1 to 0.1 V (SCE) and extending the potential range until H_2 and/or O_2 evolution evidently appeared. Figure 2 shows the final curve of BDD compared to Pt. In a compressed current scale, the differences between BDD and Pt look dramatically. O_2 evolution is shifted up to 1 V anodically and H_2 evolution up to 1 V cathodically on BDD surfaces. The "useful" potential window thus increases from *ca* 1.8 V with Pt to *ca* 3.5 V with BDD. It is clear that the surface of BDD is catalytically inert due to the lack of adsorption sites.

If the capacitive currents of Pt and BDD are compared, it is evident that they are at least one order of magnitude smaller with BDD. This is presum-

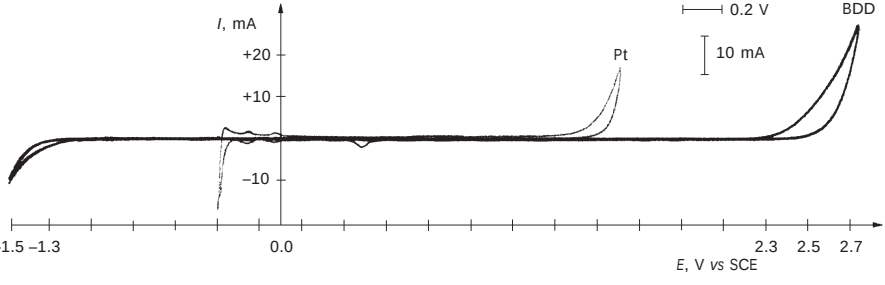

FIG. 2
Cyclic voltammetry at 100 mV s^{-1} of BDD and Pt electrodes in 0.5 M H_2SO_4 solution

ably related to the concentrations of charge carriers in BDD being substantially lower than in metals.

If the voltammetric curve of BDD is recorded on an expanded current-density scale, Fig. 3 shows that it possesses many more features than those visible in Fig. 2. In particular, a broad anodic peak before 1.8 V (SCE) is presumably related to oxidation of graphitic surface impurities. These can act as adsorption sites. Thus more and more impure samples exhibit narrower and narrower "inert" potential windows[7,9]. The oxidation of these sites (before massive O_2 evolution) is responsible for the potential plateau which settles at any current density. Therefore, the anodic pre-polarization is useful both to convert H-terminated surfaces and to "purify" the BDD surface from graphitic sites.

Figure 4 shows the cyclic voltammetric curve for one of the two RuO_2 electrodes. The shape is typically that of polycrystalline RuO_2 (ref.[18]). Also, typically, the "capacitive" current is much higher than for BDD. This is certainly due to a rougher surface of RuO_2, but also to the different mechanism of charging with oxide electrodes. Although prepared as smooth as possible, the surface charge obtained by integration amounted to *ca* 800 μC cm^{-2}, which indicates a possible roughness factor of *ca* 10, *i.e.*, one order of magnitude higher than for BDD (and Pt).

Voltammetric Curves in $[Ru(NH_3)_6]^{3+}$ Solution

The choice of the redox couple is related to its extensive use to characterize solid surfaces; it is a typical outer-sphere redox system. The electrolyte was 0.1 M $LiClO_4$ to avoid complexation with sulfuric acid.

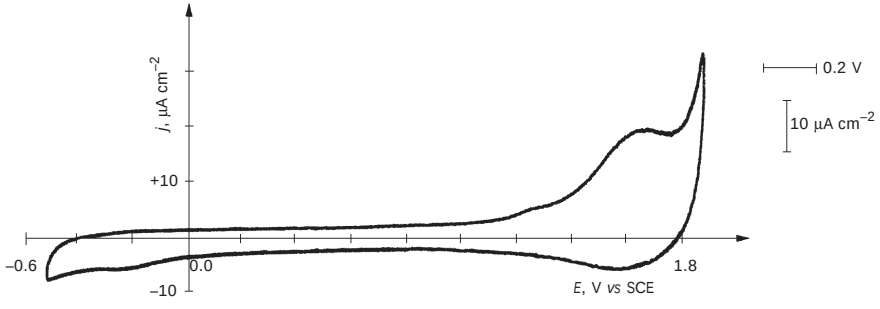

FIG. 3
The same as in Fig. 2 for a BDD electrode but in a narrower potential range with an expanded current scale

The $[Ru(NH_3)_6]^{3+/2+}$ redox couple is active around –0.2 V (SCE)[3,5,6,9]. Figure 5 shows that the CV curve of BDD in $LiClO_4$ is very flat in that potential range with absolutely no interference from other surface processes. In the case of Pt, the redox potential falls between that of hydrogen adsorption and oxide reduction, *i.e.*, more or less in the very "double layer" region. The case of RuO_2 will be discussed later.

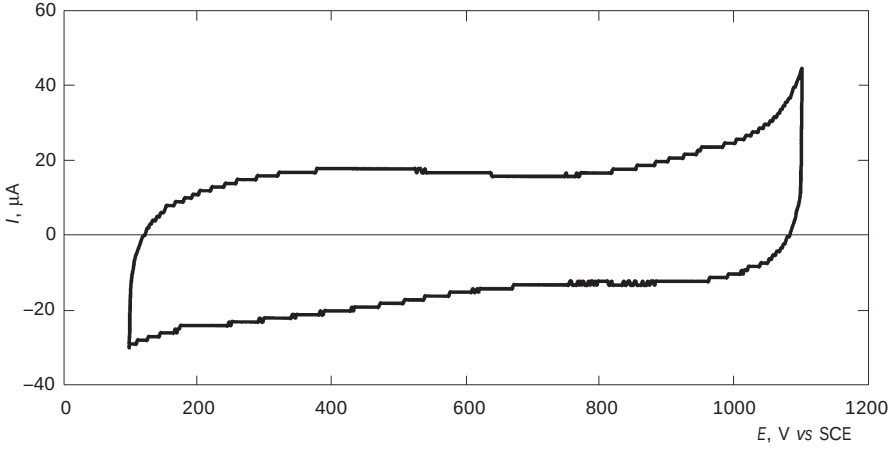

FIG. 4
Typical CV curve of a RuO_2 electrode in 0.5 M H_2SO_4 solution at 50 mV s^{-1}

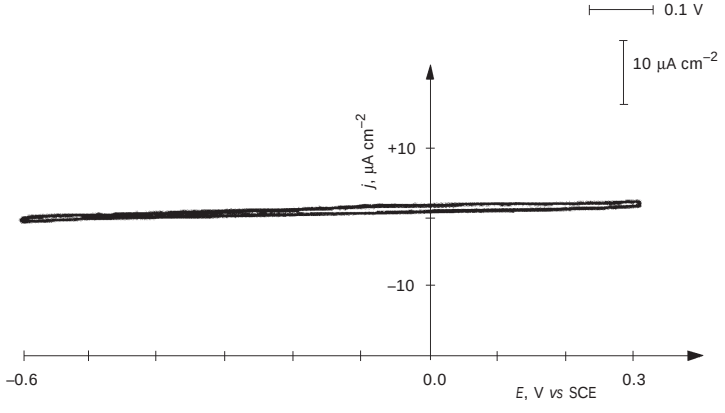

FIG. 5
Typical CV curve at 50 mV s^{-1} of BDD in 0.1 M $LiClO_4$ solution in the potential range of activity of the $[Ru(NH_3)_6]^{3+/2+}$ redox system

Figures 6–9 show the CV curves in the presence of 1 mM $[RuCl_3(NH_3)_6]$ for BDD, Pt, Au and RuO_2, respectively. At first sight, it is remarkable that all electrodes show an apparently excellent reversibility for the redox system. The only evident differences are (i) the lower peak current density for

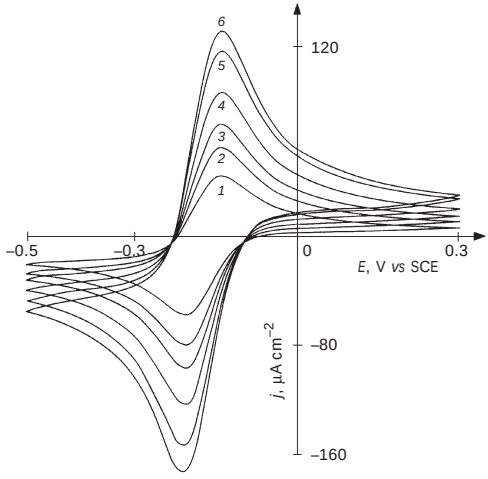

FIG. 6
CV curves of BDD electrode in 0.1 M $LiClO_4$ solution containing 1 mM $[RuCl_3(NH_3)_6]$ at various potential scan rates (in mV s^{-1}): 10 (*1*), 20 (*2*), 30 (*3*), 50 (*4*), 80 (*5*), 100 (*6*)

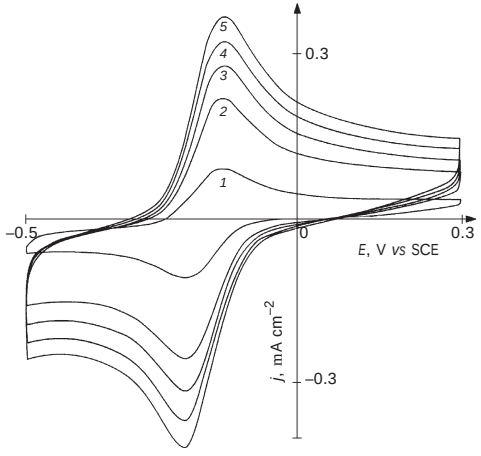

FIG. 7
CV curves at a Pt electrode in 0.1 M $LiClO_4$ solution containing 1 mM $[RuCl_3(NH_3)_6]$ at various potential scan rates (in mV s^{-1}): 20 (*1*), 100 (*2*), 150 (*3*), 200 (*4*), 250 (*5*)

BDD at a given potential scan rate, and (ii) the less evident current peak for RuO_2 due to the higher background (capacitive) current.

If the experimental data are closely scrutinized, more definite similarities and differences are brought to light. Therefore, an accurate quantitative

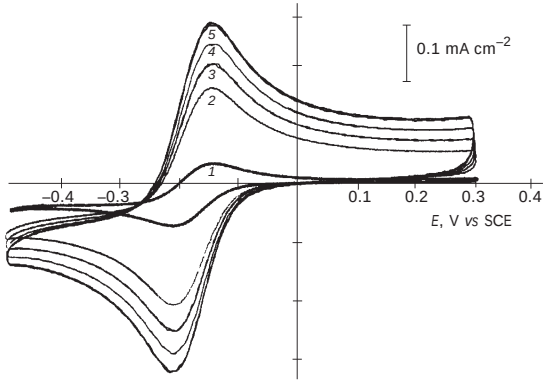

FIG. 8
CV curves of a Au electrode in 0.1 M $LiClO_4$ solution containing 1 mM $[RuCl_3(NH_3)_6]$ at various potential scan rates (in mV s^{-1}): 10 (*1*), 100 (*2*), 150 (*3*), 200 (*4*), 250 (*5*)

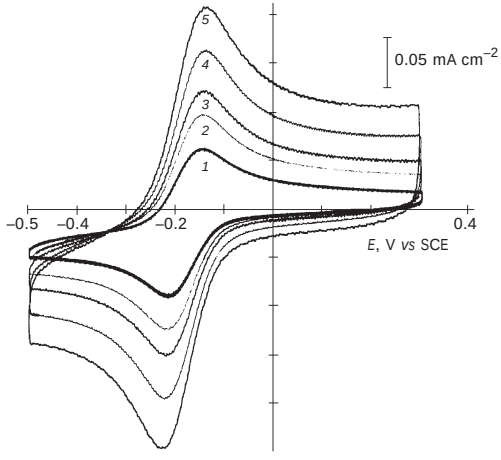

FIG. 9
CV curves of a RuO_2 electrode in 0.1 M $LiClO_4$ solution containing 1 mM $[RuCl_3(NH_3)_6]$ at various potential scan rates (in mV s^{-1}): 10 (*1*), 20 (*2*), 30 (*3*), 50 (*4*), 80 (*5*)

analysis of the reversibility criteria and of the reaction constants has been developed and reported in the next section.

Quantitative Kinetic Analysis

The assessment of the reversibility of a redox process can be based on 5 criteria:

1. I_p *vs* $v^{1/2}$, linear through the origin;
2. $\Delta E_p = E_a - E_c = 59$ mV ($n = 1$) at 25 °C;
3. I_p, $I_a/I_c = 1$;
4. E_p independent of v;
5. $E_p - E_{p/2} = 59$ mV ($n = 1$).

Tables I and II summarize the experimental parameters for BDD and Pt, respectively, necessary to check the criteria. These parameters show that the redox reaction of $[Ru(NH_3)_6]^{3+/2+}$ is almost ideally reversible on both electrodes. The same conclusion is reached also in the case of Au and RuO_2. The small deviations from ideal reversibility may be related to residual uncompensated ohmic drops or small kinetic barriers.

The calculation of k_s, the standard heterogeneous rate constant, was performed by the procedure proposed by Nicholson[19]. Accordingly, k_s can be obtained using the experimental value of ΔE_p for a given potential scan rate. The kinetic analysis of heterogeneous electron transfer leads to the definition of the quantity Ψ:

$$\Psi = (D_O/D_R)^{\alpha/2} k_s/(D_O \pi\, vF/RT)^{0.5} \quad . \qquad (1)$$

For $n = 1$, with the assumption $\alpha = 0.5$, $D_O = D_R$ and at 298 K, Eq. (*1*) becomes:

$$\Psi = k_s/0.3497 D_O{}^{1/2}\, v^{1/2} \quad . \qquad (2)$$

Equation (*1*) has been solved by Nicholson numerically thus obtaining a reference curve ΔE_p *vs* Ψ. From the experimental value of ΔE_p at a given v, a value of Ψ is derived which, from Eq. (*2*) gives k_s once D_O is known.

The value of D_O was obtained independently from the experimental dependence of I_p on $v^{1/2}$ (data for Au, with which the best reversibity was observed)[20]:

TABLE I
Experimental parameters taken from curves like those of Fig. 6 – BDD electrode[a]

ν mV/s	$\nu^{1/2}$	$E_{p,c}$ V	$E_{p,a}$ V	ΔE_p V	$E_{p,c/2}$ V	$E_{p,a/2}$ V	$\lvert E_{p,c}-E_{p,c/2}\rvert$ V	$\lvert E_{p,a}-E_{p,a/2}\rvert$ V	$j_{p,c}$ μA/cm^2	$j_{p,a}$ μA/cm^2	$\lvert j_{p,a}/j_{p,c}\rvert$	$\lvert j_{p,a}/\nu^{0.5}\rvert$ μA/cm^{2}mV$^{0.5}$	$\lvert j_{p,c}/\nu^{0.5}\rvert$ μA/cm^{2}mV$^{0.5}$
10	3.162	–0.2050	–0.1450	0.0600	–0.1525	–0.2000	0.0525	0.0550	–58	59	1.017	18.657	18.341
20	4.472	–0.2075	–0.1450	0.0625	–0.1500	–0.2000	0.0575	0.0550	–84	80	0.952	17.889	18.783
30	5.477	–0.2075	–0.1450	0.0625	–0.1475	–0.2000	0.0600	0.0550	–100	98	0.980	17.892	18.257
50	7.071	–0.2100	–0.1400	0.0700	–0.1550	–0.1975	0.0550	0.0575	–130	126	0.969	17.819	18.385
80	8.944	–0.2125	–0.1400	0.0725	–0.1450	–0.2025	0.0675	0.0625	–164	160	0.976	17.889	18.336
100	10.000	–0.2125	–0.1400	0.0725	–0.1525	–0.2000	0.0600	0.0600	–182	178	0.978	17.800	18.200
150	12.247	–0.2125	–0.1375	0.0750	–0.1575	–0.2000	0.0550	0.0625	–225	220	0.978	17.963	18.371
200	14.142	–0.2125	–0.1375	0.0750	–0.1500	–0.2000	0.0625	0.0625	–260	255	0.981	18.031	18.385
250	15.811	–0.2150	–0.1375	0.0775	–0.1525	–0.1975	0.0625	0.0600	–285	275	0.965	17.393	18.025

[a] 0.1 M $LiClO_4$ + 1 mM $[RuCl_3(NH_3)_6]$ aqueous solution.

TABLE II

Experimental parameters taken from curves like those of Fig. 7 – Pt electrode[a]

ν mV/s	$\nu^{1/2}$	$E_{p,c}$ V	$E_{p,a}$ V	ΔE_p V	$E_{p,c/2}$ V	$E_{p,a/2}$ V	$\lvert E_{p,c}-E_{p,c/2}\rvert$ V	$\lvert E_{p,a}-E_{p,a/2}\rvert$ V	$j_{p,c}$ μA/cm^2	$j_{p,a}$ μA/cm^2	$\lvert j_{p,a}/j_{p,c}\rvert$	$\lvert j_{p,a}/\nu^{0.5}\rvert$ μA/cm^{2}mV$^{0.5}$	$\lvert j_{p,c}/\nu^{0.5}\rvert$ μA/cm^{2}mV$^{0.5}$
10	3.162	–0.2025	–0.1450	0.0575	–0.1450	–0.1950	0.0575	0.0500	–70	70	1.000	22.136	22.136
20	4.472	–0.2000	–0.1400	0.0600	–0.1475	–0.1950	0.0525	0.0550	–100	100	1.000	22.361	22.361
30	5.477	–0.2025	–0.1425	0.0600	–0.1500	–0.2050	0.0525	0.0625	–115	115	1.000	20.996	20.996
50	7.071	–0.2075	–0.1425	0.0650	–0.1500	–0.1950	0.0575	0.0525	–150	150	1.000	21.213	21.213
80	8.944	–0.2075	–0.1425	0.0650	–0.1475	–0.1950	0.0600	0.0525	–200	190	0.950	21.243	22.361
100	10.000	–0.2075	–0.1400	0.0675	–0.1500	–0.1925	0.0575	0.0525	–215	200	0.930	20.000	21.500
150	12.247	–0.2075	–0.1350	0.0725	–0.1475	–0.1925	0.0600	0.0675	–260	245	0.942	20.004	21.229
200	14.142	–0.2100	–0.1350	0.0750	–0.1500	–0.1950	0.0600	0.0600	–300	285	0.950	20.153	21.213
250	15.811	–0.2125	–0.1375	0.0750	–0.1450	–0.1925	0.0675	0.0550	–340	320	0.941	20.239	21.503

[a] 0.1 M $LiClO_4$ + 1 mM $[RuCl_3(NH_3)_6]$ aqueous solution.

$$I_p = 2.69 \times 10^5 A D_O^{1/2} v^{1/2} c_O \,, \qquad (3)$$

where A is the electrode surface area and c_O the concentration of the oxidized species. Thus, the value $D_O = 6.3 \times 10^{-6}$ cm^2 s^{-1} has been obtained. In principle, according to Eq. (*3*), D_O might depend on the electrode material. D_O is however a constant in these calculations, and cannot influence the relative behavior of the different materials.

Table III summarizes the calculated values of k_s for Pt, Au, BDD and RuO_2. The accuracy of the calculations were checked numerically. There are two possible sources of error: the value of ΔE_p and the interpolated value of Ψ. While the interpolation of Ψ has minor effects (*e.g.*, at 20 mV s^{-1}, k_s can vary between 0.035 and 0.043 cm s^{-1} for BDD), the value of ΔE_p can have a higher impact since it depends on the position of ΔE_p on the ΔE_p *vs* Ψ curve. Thus, as an example, k_s can vary between 0.015 and 0.048 cm s^{-1} for BDD at 30 mV s^{-1}, while at same value of v, the range is only 0.005–0.006 for RuO_2. In other words, inaccuracies in the determination of the experimental parameters cannot overturn the resulting kinetic picture. Thus, the data in Table III are comparatively significant.

The data in Table III highlight two main points: (i) The values of k_s are of the same order of magnitude, mostly very similar, for Au, Pt and BDD. The last material "appears" only marginally less "metallic" than Pt and Au, which behave in practically the same way. (ii) The value of k_s for RuO_2 is *ca*

TABLE III
Standard rate constant (k_s, cm s^{-1}), for the $[Ru(NH_3)_6]^{3+/2+}$ redox system on different electrode materials

v, mV s^{-1}	Pt	Au	BDD	RuO_2
50	0.031	0.031	0.020	0.005
80	0.039	0.025	0.018	0.005
100	0.028	0.020	0.020	0.005
150	0.020	0.025	0.020	0.005
200	0.021	0.023	0.021	0.005
250	0.023	0.026	0.023	0.005
Mean	0.027	0.025	0.020	0.005

one order of magnitude smaller. Since the resistivity of RuO_2 is lower than that of BDD, such a difference cannot be related to the different electronic band structure. If $[Ru(NH_3)_6]^{3+/2+}$ behaves really as an outer sphere system, the lower value of k_s can be attributed to a larger distance between the solid surface and the reacting ion in solution. This idea fits well with the known structure of an oxide/solution interface[21] where water layers are strongly held by the hydrophilic forces of the oxide surface. In this context, the reacting ion can be well impeded by the adsorbed water layer to come closer to the solid electrode surface.

CONCLUSIONS

For the first time electron transfer reactions at BDD, a native hydrophobic surface, are compared with RuO_2, a strongly hydrophilic surface. The outcome is that the electron exchange rate is lower on RuO_2, despite its metallic conductivity. This is taken as an indication of an increase in the tunneling distance for electron transfer due to strongly held water layers on the oxide surface.

On the other hand, the electron exchange rate is almost the same on BDD, Pt and Au. Since in the case of Au, complications due to adsorbed oxygen are minimized, the results indicate that pre-anodization of the BDD surface does not change irremediably the pristine hydrophobic character of its surface, so that outer sphere electron transfer is still possible without observable hindrance. The situation may change with a different redox couple.

Our thanks are due to the financial support of MIUR (Cofin) and C.N.R.

REFERENCES

1. Maeda Y., Sato K., Ramaraj R., Rao T. N., Tryk D. A., Fujishima A.: *Electrochim. Acta* **1999**, *44*, 3441.
2. Beck F., Kaiser W., Krohn H.: *Electrochim. Acta* **2000**, *45*, 4691.
3. Sunkara M. K., Koduri P., Dickey E. C., Fan X.: *Electrochem. Soc. Proc.* **1999**, *99-32*, 448.
4. Pleskov Yu. V., Evstefeeva Yu. E., Krotova M. D., Laptev A. V.: *Electrochim. Acta* **1999**, *44*, 3361.
5. Vinokur N., Miller B., Avyigal Y., Kalish R.: *J. Electrochem. Soc.* **1996**, *143*, L238.
6. Goeting C. H., Jones F., Food J. S., Eklund J. C., Marken F., Compton R. G., Chalker P. R., Johnston C.: *J. Electroanal. Chem.* **1998**, *442*, 207.
7. Strojek J. W., Granger M. C., Swain G. M., Dallas T., Holtz M. W.: *Anal. Chem.* **1996**, *68*, 2031.

8. Yagi I., Notsu H., Kondo T., Tryk D. A., Fujishima A.: *J. Electroanal. Chem.* **1999**, *473*, 173.
9. Alehashem S., Chambers F., Strojek J. W., Swain G. M., Ramesham R.: *Anal. Chem.* **1995**, *67*, 2812.
10. Ferro S., De Battisti A.: *J. Electroanal. Chem.* **2002**, *533*, 177.
11. Ferro S., De Battisti A.: *Electrochim. Acta* **2002**, *47*, 1641.
12. Ferro S., De Battisti A.: *Phys. Chem. Chem. Phys.* **2002**, *4*, 1915.
13. Garavaglia R., Mari C. M., Trasatti S.: *Surf. Technol.* **1984**, *23*, 41.
14. Lodi G., Sivieri E., De Battisti A., Trasatti S.: *J. Appl. Electrochem.* **1978**, *8*, 135.
15. Notsu H., Yagi I., Tatsuma T., Tryk D. A., Fujishima A.: *Electrochem. Solid State Lett.* **1999**, *2*, 522.
16. Duo I., Michaud P.-A., Haenni W., Perret A., Comninellis Ch.: *Electrochem. Solid State Lett.* **2000**, *3*, 325.
17. Ferro S., De Battisti A., Duo I., Comninellis Ch., Haenni W., Perret A.: *J. Electrochem. Soc.* **2000**, *147*, 2614.
18. Trasatti S., Buzzanca G.: *J. Electroanal. Chem.* **1971**, *29*, App. 1.
19. Nicholson R. S.: *Anal. Chem.* **1965**, *37*, 1351.
20. Bard A. J., Faulkner L. R.: *Electrochemical Methods*. Wiley, New York 1980.
21. Ardizzone S., Trasatti S.: *Adv. Colloid Interface Sci.* **1996**, *64*, 173.